

# Practical polarization-frame alignment for quantum key distribution with single-photon-level resources

Brendon L. Higgins,\* Jean-Philippe Bourgoin, and Thomas Jennewein

*Institute for Quantum Computing, University of Waterloo, Waterloo, Ontario N2L 3G1, Canada and  
Department of Physics and Astronomy, University of Waterloo, Waterloo, Ontario N2L 3G1, Canada*

When quantum information is encoded in optical polarization, practical protocols must contend with the fact that preparation and measurement reference frames may be misaligned, owing to physical orientations and birefringence effects. For long-distance transmissions, a common solution involves multiplexing strong classical reference signals, providing a basis for correction. Here we numerically investigate the performance of a polarization-frame alignment protocol utilizing single-photon-level signals and measurements, in the context of quantum key distribution (QKD) over channels with detector noise and imperfect sources. To the extent possible, the same states and measurement bases are used as for the QKD protocol we intend to support. Our results show that a small fraction of resources from the overall signal—a few hundred photon detections, in total—are required for good performance, restoring the state to better than 99% of its original quality, and we illustrate the protocol’s successful operation and adaptability through experimental demonstrations in which it was used in the laboratory and the field.

## I. INTRODUCTION

Quantum communications technologies promise to be exciting new avenues for disseminating, processing, and controlling information. The most commercially ready of these technologies, quantum key distribution (QKD), distills a secure encryption key from the measurement results of quantum states sent from one party, Alice, to another, Bob, via a quantum channel [1, 2]. In particular, BB84 [3] and related QKD protocols utilize the no-cloning theorem on qubit states to guarantee that an eavesdropper cannot ascertain any bits of the key without introducing detectable noise into the measurement statistics.

Optical platforms are an obvious choice for communicating quantum information, and one common information carrier is the electromagnetic-field polarization of photonic states. However, optical polarization denotes a direction in space, and for many quantum communications protocols, such as polarization-encoded BB84, the relative alignment of Alice’s and Bob’s polarization reference frames is crucial to the protocol’s serviceability. Ensuring such alignment can be challenging for long-distance transmissions, such as between the ground and an orbiting satellite platform [4], or through fiber-optic cables between distant sites.

For protocols that rely on faithful transmission of qubit states over a quantum channel, the orientation and phase of each transmitted state must be preserved. This poses a problem beyond spatial frame alignment (see also [5]) for birefringent media, such as optical fibers. The accumulating effect of birefringence in optical fiber transmission, dependent on temperature, physical coiling of the fiber, and the wavelength of the signal, introduces unpredictable rotations of the polarization state that can

be around any axis on the Poincaré sphere.

A number of frame-alignment schemes for quantum systems have been investigated which aim for optimal outcomes, under particular constraints, by employing multi-photon collectively-entangled states and/or measurements (see, e.g., [6–11]). Implementing these is difficult in practice, and such schemes tend to scale poorly with distance due to the losses acting upon each photon within these collective systems. A more practical approach is to augment quantum communications protocols to be reference-frame independent (RFI), such that they utilize polarization subspaces in a way that is insusceptible to specific issues—for example, utilizing the invariance of the circular polarization basis under physical rotations around the beam path (but not birefringence-induced phase effects) for QKD [12–15]. Another approach applies a generic compensation based on measurements of a correlated side-channel, such as polarimetry of a strong, classical signal multiplexed into the fiber at times or wavelengths near (but distinguishable from) the quantum signal [16, 17].

Despite the above, a question remains: what resources are required for frame alignment if one is limited only to separable, single-qubit states and measurements, such as those used as standard in BB84 QKD and alike protocols? Here we examine a polarization frame alignment protocol that operates using such quantum signals and straightforward analysis and optimization techniques to correct arbitrary polarization rotations in the transmission channel. We quantify the number of photons required for high-fidelity correction of the polarization states by performing numerical simulations, and show excellent correction based on only a small fraction of the received photon detections in a realistic environment possessing noise and imperfect source visibility. We further present examples of use of this alignment protocol in laboratory and field QKD experiments.

This paper is organized as follows: Section II details the two stages of the alignment protocol in nominal (post-

---

\* brendon.higgins@uwaterloo.ca

compensating) and alternative (pre-compensating) configurations. Section III presents the numerical simulations we performed of this protocol in both configurations, and Sec. IV briefly shows some results from a variety of laboratory and field tests in which the protocol was put to use. In Sec. V we note how the ambiguity between timing and polarization frame misalignment at initialization can be solved in practical contexts, and finally give concluding remarks in Sec. VI.

## II. POLARIZATION ALIGNMENT PROTOCOL

As we aim to support polarization-encoded QKD, we assume that there are no significant polarization-sensitive *non*-unitary effects within the quantum channel [18]. For photons that successfully traverse the channel, the most significant effects on polarization—owing to birefringence and physical orientation—can then be characterized as  $SU(2)$  rotations of the polarization-encoded qubit state. Although these effects may arise from various sources, any combination of them can be described as a quantum channel applying a single  $SU(2)$  unitary  $\hat{U}$  to any state sent from Alice and received by Bob. This allows us to use a consistent polarization frame—namely, Alice’s—for the entirety of the treatment that follows.

We conceptually separate the alignment protocol into two main tasks: (a) characterize the action of the channel such that it has sufficient information about  $\hat{U}$  to then (b) determine, and subsequently implement, a compensation operation  $\hat{V}$  such that the combined action of  $\hat{U}$  and  $\hat{V}$  closely approximates identity.

### A. Characterization

The effect of the quantum channel is characterized by transmitting a predefined set of states through the channel and analyzing measurement outcomes. Let  $|\psi_{a,n}\rangle$  be one such transmitted state, with  $|\psi_{b,n}\rangle = \hat{U}|\psi_{a,n}\rangle$  being the corresponding state measured at the receiver.

Given a measurement eigenstate  $|\phi_m\rangle$ , the fidelity after applying the unknown unitary,  $F(\phi_m|\psi_{b,n}) = |\langle\phi_m|\psi_{b,n}\rangle|^2$ , quantifies the probability of obtaining that measurement outcome. We note that, in most practical situations, this is limited by an intrinsic signal fidelity,  $F_S$ , owing to imperfections of source, channel, and measurement apparatuses leading to real or apparent depolarization. We can encompass these into an effective state  $\hat{\rho}_n = (2F_S - 1)|\psi_{b,n}\rangle\langle\psi_{b,n}| + (1 - F_S)\hat{I}$  being measured at the receiver after the unknown unitary of the channel is applied, with  $\hat{I}$  being the identity operator. For the following, we assume  $F_S \rightarrow 1$ .

To completely determine the action of  $\hat{U}$ , it is sufficient to accurately characterize the direction of one post- $\hat{U}$  state vector and the residual angular rotation about that vector. In practice we can satisfy this by transmit-

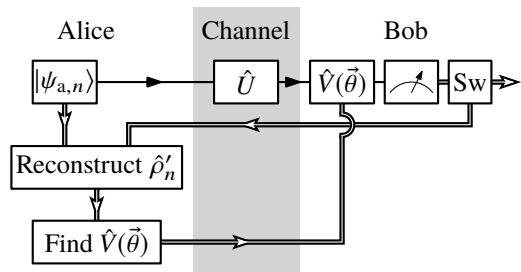


FIG. 1. Schematic overview of the polarization alignment protocol as considered here. In this “forward” configuration, Alice prepares states  $|\psi_{a,n}\rangle$  and transmits them to Bob, with the channel imparting an unknown unitary rotation  $\hat{U}$ . Ordinarily, the states are measured at Bob and the results are utilized by the quantum communication protocol (generating raw key bits, in the case of QKD). For characterization, Bob measures the states in a tomographically complete basis set—potentially making use of the controllable unitary  $\hat{V}(\vec{\theta})$  to do so—with a data path switch (Sw) directing the results back to Alice. (A switch could alternatively be placed prior to measurement, allowing unmeasured qubits to pass downstream.) The detection coincidence counts are used to reconstruct the received states  $\hat{\rho}'_n$  for each  $n$ .  $\vec{\theta}$  are then optimized in a numerical model of compensation optics,  $\hat{V}(\vec{\theta})$ , and finally applied to the real apparatus for compensation of subsequent transmissions. A “reversed” configuration can be similarly constructed where  $\hat{V}(\vec{\theta})$  is applied before the qubit traverses the quantum channel.

ting ensembles of (at least) two different, non-orthogonal states (say,  $|\psi_{a,1}\rangle$  and  $|\psi_{a,2}\rangle$ ),

followed by single-qubit state tomography (i.e., single-photon polarimetry) of these states at the receiver.

We focus our attention on the  $|H\rangle$ ,  $|V\rangle$ ,  $|D\rangle = (|H\rangle + |V\rangle)/\sqrt{2}$ , and  $|A\rangle = (|H\rangle - |V\rangle)/\sqrt{2}$  states prepared as part of the BB84 QKD protocol. If Bob’s apparatus is sufficient to perform single-qubit state tomography, Alice may simply continue transmitting the same random sequence of states in  $|H\rangle$ ,  $|V\rangle$ ,  $|D\rangle$ , and  $|A\rangle$  (defining  $|\psi_{i,n}\rangle$  for  $n \in \{1, 2, 3, 4\}$ , respectively) [19]. Temporal correlation of photon measurement events to the corresponding input states (i.e., particular values of  $n$ ) can be performed using the same procedures Alice and Bob must already utilize for QKD (but see Sec. V). This allows photon measurement counts for each  $n$  to be collected even though these states are sent in random order.

The four BB84 input states are indeed more than necessary for complete characterization of  $\hat{U}$ —the states  $|H\rangle$  and  $|D\rangle$  alone would be sufficient. The detection counts corresponding to the extra states orthogonal to each of these could be simply discarded, in principle, but in practice the measurement results are easily included in analysis and compensation (see below), and doing so maintains a high efficiency of the polarization alignment protocol while requiring minimal changes to the QKD apparatus.

Tomographic reconstruction of each state  $|\psi_{b,n}\rangle = \hat{U}|\psi_{a,n}\rangle$  is then based on time-correlated photon detec-

tion statistics. Like the transmitted states, for practicality it makes most sense to utilize the measurement outcome eigenstates Bob already utilizes to implement BB84 ( $|H\rangle$ ,  $|V\rangle$ ,  $|D\rangle$ , and  $|A\rangle$ ). Thus, for tomography, we use the tomographically complete set of measurements defined by the three Pauli matrices  $\hat{Z}$  (projecting into  $|H\rangle/|V\rangle$ ),  $\hat{X}$  (projecting into  $|D\rangle/|A\rangle$ ), and  $\hat{Y}$  (projecting into  $|R\rangle/|L\rangle$ , where  $|R\rangle = (|H\rangle + i|V\rangle)/\sqrt{2}$ , and  $|L\rangle = (|H\rangle - i|V\rangle)/\sqrt{2}$ ). In fact, this set of measurements is tomographically overcomplete, in the sense that they are more than necessary to extract full state information. Even so, measurements in the circular polarization basis,  $|R\rangle/|L\rangle$ , are necessary (states lying only on a great circle of the Poincaré sphere, such as BB84 states, are not tomographically complete), placing an additional requirement on Bob’s apparatus beyond BB84 QKD. As we see below, the compensation mechanism can itself be utilized to achieve a change of basis necessary to implement these projections without further modifications, such as additional detectors, to Bob’s receiver.

The overcomplete basis set provides additional experimental robustness when compared to a complete basis set [20] and, because most of these bases are also the BB84 measurement bases, can be practically implemented at the receiver. For each  $n$ , we tomographically reconstruct the density matrix  $\hat{\rho}'_n$  from measured counts in these bases using maximum likelihood estimation [21]. With these density matrices, an appropriate compensation can then be determined.

## B. Compensation

We consider a compensation of the unitary  $\hat{U}$  taking place at the receiver just prior to measurement. Any  $SU(2)$  operation can be implemented in polarization optics by a quarter-, half-, quarter-wave plate arrangement, the operation being parametrized by the physical rotation of the three wave plates from their optic axes around the beam path. Determining the optimal compensation is thus a matter of optimizing the three wave plate orientation angles  $\vec{\theta} = (\theta_1, \theta_2, \theta_3)$  such that each in the set of characterized states (each  $|\psi_{b,n}\rangle$ ) matches the corresponding transmitted state ( $|\psi_{a,n}\rangle$ ) with high fidelity.

For our implementation, we utilize the common Nelder–Mead simplex optimization algorithm. First, we construct a theoretical compensation unitary  $\hat{V}(\vec{\theta}) = \hat{Q}(\theta_3)\hat{H}(\theta_2)\hat{Q}(\theta_1)$  encompassing the operation of the three wave plates given the parameters  $\vec{\theta}$ . The cost function of the algorithm,  $C$ , is then defined as the negative sum of fidelities between each predicted state, after applying the compensation operation, and the corresponding initial state—i.e.,

$$C = - \sum_n \langle \psi_{a,n} | \hat{V}(\vec{\theta}) \hat{\rho}'_n \hat{V}^\dagger(\vec{\theta}) | \psi_{a,n} \rangle. \quad (1)$$

(Here we employ a more general form of fidelity to ac-

commodate the density matrix  $\hat{\rho}'_n$ , which may not be a pure state.)

If the reconstructed states  $\hat{\rho}'_n$  accurately characterize the measured states  $|\psi_{b,n}\rangle$  (i.e., if  $\hat{\rho}'_n \approx \hat{U} |\psi_{a,n}\rangle \langle \psi_{a,n}| \hat{U}^\dagger$ ), then the cost function  $C$  will be minimized when  $\hat{V}(\vec{\theta})\hat{U} = \hat{I}$ , the identity operator. Minimizing  $C$  by varying  $\vec{\theta}$  (as dictated by the minimization algorithm) thus optimizes the compensation operation. Applying the optimized theoretical wave plate orientations  $\vec{\theta} = (\theta_1, \theta_2, \theta_3)$  to actual wave plates at the receiver implements the compensation and completes the alignment protocol [22].

Note that in the above formalism we have assumed, for simplicity, that while photon counting for characterization of  $\hat{U}$  is taking place, the compensation wave plates are set such that they implement the identity operation  $\hat{I}$  (e.g., by moving back to their optic axes). However, the effect of the wave plates not being at their optic axes during this phase, assuming their positions are known, can be straightforwardly incorporated. In addition, they can be also used for a secondary purpose if Bob’s apparatus is only capable of photon counting in the  $\hat{Z}$  and  $\hat{X}$  bases. There, the compensation wave plates can be utilized to implement a change of basis prior to the state projection, and thereby achieve projections onto circular polarizations. (This could be done by, e.g., setting the second quarter-wave plate to an angle  $45^\circ$  from its optic axis, effectively transforming  $\hat{Z}$  into  $\hat{Y}$  for the remaining measurement time.)

## C. Reversal using post-selection

Typically, the compensation wave plates would be mounted in motorized rotation stages at the receiver, but for some situations it may be more suitable for these components to be placed at the transmitter. For example, such moving parts on an orbiting satellite platform introduce undesirable complexity, making the protocol problematic for a satellite receiver platform [23]. To address this, we exploit the time-symmetric nature of quantum mechanics to construct a “reversed” version of the above “forward” algorithm. Here, measurements of transmitted states are classified in a manner akin to post-selection, allowing us to establish an optimal pre-compensation operation that is applied to the photons immediately before leaving the transmitter.

Compared to the forward version of the protocol, in this reversed version the sets of input and measured states are swapped—for example, we define  $|\psi_{a,n}\rangle \in \{|H\rangle, |V\rangle, |D\rangle, |A\rangle, |R\rangle, |L\rangle\}$ , and  $|\phi_m\rangle \in \{|H\rangle, |V\rangle, |D\rangle, |A\rangle\}$ . As before, measurement count statistics are collected for each combination of input and measured state. Let  $d_{nm}$  be the counts for each input state index  $n$  and measurement outcome index  $m$ . For each  $m$ ,  $d_{nm}$  covers a set of input states that forms a tomographically complete (in fact, overcomplete) basis set.

By selecting the counts  $d_{nm}$  for a fixed  $m$  and performing tomography using those counts—i.e., over all the transmitted states, for each outcome—we reconstruct the effective input state conditional on post-selecting  $|\phi_m\rangle$ . In other words, we thus determine (up to the imprecision of the tomographic reconstruction) what states Alice would have sent Bob in order for them to become  $|\phi_m\rangle$  upon application of the unknown unitary  $\hat{U}$ . The compensation is then optimized in the same manner as the forward protocol.

### III. MONTE CARLO NUMERICAL SIMULATIONS

To determine the performance characteristics of the alignment protocol, we conduct a series of numerical simulations incorporating a Haar-distributed random unitary  $\hat{U}$ , stochastic count generation, the characterization (tomography) and compensation (optimization) components of the protocol, virtual compensating wave plate operations, and resulting fidelity assessment. Using this, we perform a large number of Monte Carlo simulations of the protocol in both forward and reversed configurations.

For QKD, the primary goal is reducing the quantum bit error ratio (QBER),  $E$ , which quantifies the ratio of unexpected measurement outcomes to the total (within each basis relevant for QKD), and is used to determine the security of the channel. A lower QBER allows the bandwidth of key distribution to be increased, while a high QBER can cause the QKD protocol to be aborted with no secure key generated. The QBER is intimately related to the fidelities of the received states—specifically,  $E = 1 - \sum_n F_n/4$ , where  $F_n$  is the measured fidelity of the received state  $\hat{\rho}_n$  against the expected  $|\phi_n\rangle$ . In the context of our compensation algorithm, it is straightforward to show that the QBER  $E$  and cost function  $C$  are linearly related, with minimal  $C$  implying minimal  $E$ , so long as  $\hat{\rho}'_n$  is a sufficiently accurate estimate of  $\hat{\rho}_n$ .

We quantify the polarization alignment protocol’s performance from our simulation results using the mean predicted QBER,  $\bar{E}$ , of the nominal (ideal) signal states after the application of the channel unitary  $\hat{U}$  followed by the compensation unitary  $\hat{V}(\vec{\theta})$ . With this definition, this “residual” QBER is zero for perfect compensation, regardless of the actual intrinsic signal fidelity  $F_S$ .

We independently vary the number of detected photons  $N$  and the intrinsic signal fidelity  $F_S$ . Our results are calculated from  $2^{24} \approx 16.8$  M samples of the Monte Carlo simulation for each of a total 468 configurations. From these results we obtain very good estimates of the expected mean residual QBERs and their standard deviations.

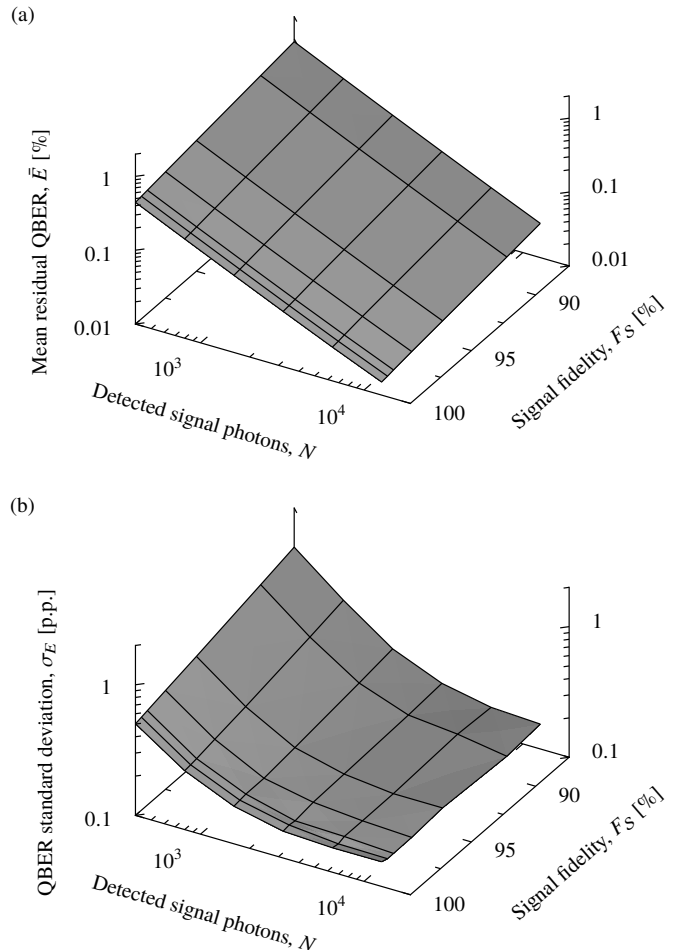


FIG. 2. Performance of the forward polarization alignment protocol. (a) Mean residual QBER of nominal signal states after optimized compensation based on characterization analysis of  $N$  detected signal photons with intrinsic signal fidelity  $F_S$  at the receiver. Only a few hundred photons are required to achieve low mean QBER. (b) Standard deviation of the QBER. Low photon counts and low intrinsic signal fidelities significantly increase the variation of performance between applications of the protocol.

#### A. Forward protocol

The results for the forward protocol are illustrated in Fig. 2(a). Given reception of a signal with perfect intrinsic fidelity, the mean residual QBER owing to the application of the polarization alignment protocol is less than 0.5% when at least  $N = 400$  photons are measured (an average of 100 photons per input state, the lowest simulated), reducing to less than 0.016% for 12 800 photons. (These values are consistent with common understanding that a few thousand copies are sufficient for producing good qubit state estimates via tomography [24].) In other words, in this condition, as few as four hundred detections are sufficient to recover over 99.5% fidelity when an unknown unitary is being applied.

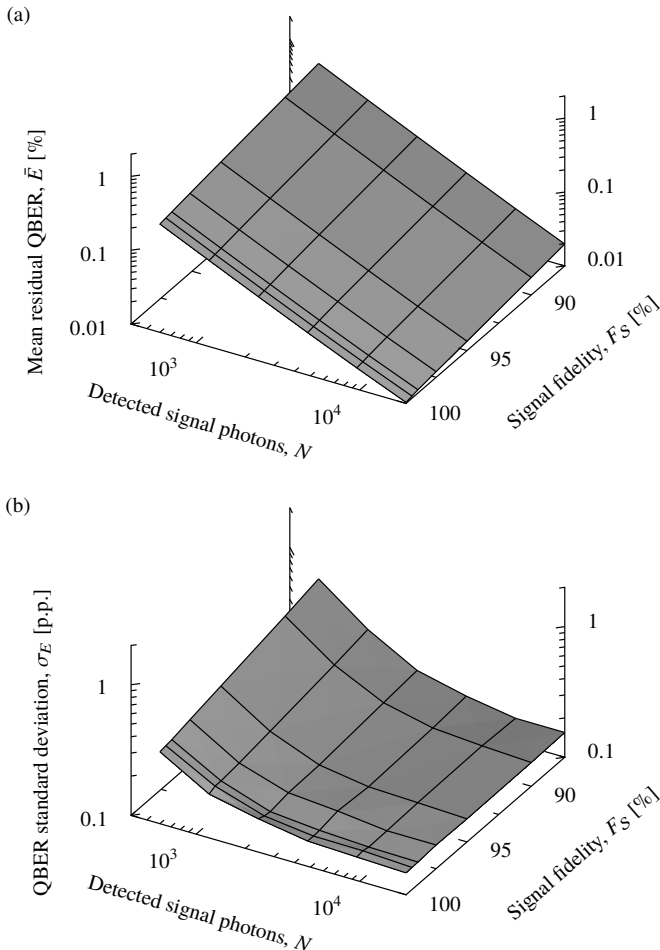


FIG. 3. Performance of the reversed polarization alignment protocol. Subfigures (a) and (b) are as in Fig. 2.

For QKD, the expected detection rate for a weak coherent pulse (WCP) source is  $R[1 - (1 - Y_0)e^{-\eta\mu}]$ , where  $R$  is the source pulsing rate,  $\mu$  is the coherent state mean photon number,  $\eta$  is the transmission of the channel, and  $Y_0$  is the vacuum yield (per pulse) at the receiver. Neglecting the vacuum yield, for typical WCP source parameters— $\mu = 0.5$  at  $R = 300$  MHz—the expected detection rate over a channel with a significant 40 dB loss will be  $\approx 15$  kHz. Of this, 400 detections would be less than 3% of one second of data collection—less than some implementations reveal for the purpose of parameter estimation. (In fact, such revealed parameter-estimation outcomes could be utilized for polarization characterization.) Contrast this also to correction techniques based on classical polarimetry, which utilize many orders of magnitude more photons.

In the more realistic condition where the measured signal has imperfect intrinsic fidelity, the mean residual QBER is exacerbated—for example, for 95% intrinsic signal fidelity, 400 detections leads to 0.59% mean residual QBER, resulting from the inherent statistical uncertainty. A signal with at least  $F_S \approx 87.5\%$  intrinsic

fidelity is necessary to maintain less than 1% mean residual QBER for 400 photons. Note that this intrinsic signal fidelity corresponds to an intrinsic signal QBER of at least 12.5%—too high to perform successful QKD, but evidently enough for good correction of  $\hat{U}$ . For comparison, good sources for QKD produce signals with fidelities approaching, sometimes exceeding, 99%. (In the context of a satellite receiver, background and detector dark counts are expected to be the largest contributor to the imperfect intrinsic fidelity of the measured signal [23].)

We perform a least-squared-error fit of the results of the simulation to a function of the form  $\bar{E}(F_S, N) = \alpha(2F_S - 1)^\beta N^\gamma$ . The optimized values,  $\alpha \approx 2.93$ ,  $\beta \approx -2.23$ , and  $\gamma \approx -1.07$ , yield a coefficient of determination of 0.9999, in excellent agreement with the data. In addition, the value of  $\gamma$  corresponds quite well with the expected  $1/N$  precision scaling of the tomographic reconstruction, suggesting that the tomography—necessary for characterizing the unitary—may be the limiting factor in the precision of the polarization alignment protocol.

Figure 2(b) shows the standard deviation of the residual QBER after compensation, illustrating the variability in the outcomes of each run. Given low numbers of photon detections, a drop in the intrinsic signal fidelity results in significant variations, exceeding one percentage point (p.p.) for  $F_S = 87.5\%$  (and worse for lower  $F_S$  values not shown), in the resulting residual QBERs of the protocol. With high intrinsic signal fidelity, however, the protocol behaves consistently, with standard deviations no more than about one-half of a percentage point.

## B. Reversed protocol

The reversed protocol is also simulated, with results plotted in Fig. 3. As with the forward protocol, the general trend of better performance (lower mean residual QBER) with better intrinsic signal fidelity and higher numbers of detected photons is maintained. The overall performance, and variability, is very similar to the forward protocol. For example, with  $N = 600$  measured photons (again, 100 photons per input state) and an intrinsic signal fidelity  $F_S$  of 95%, we find the reversed protocol achieves 0.39% mean residual QBER, comparable to the forward protocol. We again perform a least-squared-error fit to the function  $\bar{E}(F_S, N) = \alpha(2F_S - 1)^\beta N^\gamma$ , this time resulting in optimized values  $\alpha \approx 3.25$ ,  $\beta \approx -2.22$ , and  $\gamma \approx -1.08$ , and yielding a coefficient of determination of 0.9998.

## C. Ineffectiveness of background subtraction

To try to improve the protocol under realistic use cases, we perform some additional simulations exploring the utility of a simple background noise removal strategy. For these simulations we add random (Poissonian) background counts to the simulated detected counts and then

subtract the mean background (while guarding against unphysical negative counts) prior to the characterization step. The intent is to examine the effectiveness of subtracting a known (e.g., pre-calibrated) background level from the measurements to improve the signal-to-noise ratio.

For various photon detection counts  $N$  and intrinsic signal fidelities  $F_S$ , we compare the residual QBER of the alignment protocol operating with background subtraction,  $\bar{E}_{BGS}$ , against the alternative case where the background counts are added but the mean not subtracted,  $\bar{E}_{BG}$ . The results indicate that background subtraction is not better, and in many conditions clearly worse, than leaving the counts with background unaltered. This is illustrated by Fig. 4, which shows the increase of the residual QBER found when subtracting background (i.e.,  $\bar{E}_{BGS} - \bar{E}_{BG}$ ) in both forward and reversed cases.

#### IV. IMPLEMENTATIONS IN LABORATORY AND FIELD TRIALS

Our polarization alignment protocol has been utilized in various manners to maintain the stability of the quantum channel of several experimental QKD demonstrations. The first was in the context of high-loss QKD experiments [25]. Here, the WCP source employed up-conversion (sum frequency generation, or SFG) of a mode-locked 810 nm Ti:sapphire laser (76 MHz pulse rate) with a 1550 nm polarization-modulated continuous-wave telecom laser. Polarization modulation was achieved using a fiber-based balanced Mach-Zehnder interferometer (MZI) with a high-speed electro-optic phase modulator in each interferometer arm [26]. Optical fibers guided the telecom pulses from the laser through the interferometer, as well as the 532 nm QKD signal SFG output to the transmitter (the remainder of the quantum channel was free space).

While multi-hour stability of the polarization state generation was observed, the interferometer and optical fibers were sensitive to local temperature fluctuations and had significant settling time after any manipulations of the apparatus. The result of such effects on the measured QBER at Bob is illustrated in Fig. 5, where measurements were taken over several hours. At two points during this test, when the QBER was noticed to have drifted particularly high, the polarization alignment protocol was engaged. In this implementation, the compensating wave plates were used to effect a change of basis. As discussed previously, this allowed all three bases to be measured by the apparatus' four detectors nominally configured for rectilinear polarization bases. As this was an early test of the polarization alignment system, for certainty  $\approx 140\,000$  detection events were used for characterization. After the optimized rotation angles were applied to the compensation wave plates (in motorized stages), the QBER returned to the intrinsic level of  $\approx 2\%$ , indicating that the protocol corrects polarization

rotations as intended.

Subsequent work sought to perform QKD from a transmitter at a fixed location to a receiver in the bed of a moving truck [27]. To facilitate this, both transmitter and receiver were placed on 2-axis motorized rotation stages for pointing. While the state analysis elements of the receiver apparatus were all placed on the moving stage,  $\approx 85$  m of single-mode optical fiber guided QKD states from the source in a temperature-controlled laboratory, through the core of the building, to the transmitter on the pointing stages located in an open-air dome on the building's roof. With such a long fiber, continuous movement and temperature fluctuations dominated contributions to the QBER, necessitating an *active* polarization correction method to reliably maintain performance throughout testing. To achieve this, the polarization alignment protocol was automated so that photon counts were analyzed and wave plate angles optimized once every second.

As the receiver in the truck was expected to remain closely physically oriented with respect to the transmitter, for simplicity the per-second polarization alignment protocol was applied only at Alice's side to correct rotations from the source up to the free-space link—from the perspective of the polarization alignment protocol, Bob was located just prior to the transmitter telescope. (In principle, the compensation optimization could be extended to incorporate a physical orientation between the transmitter and receiver if this information was given by, for example, attitude monitors.) In the picture of Fig. 1, the classical channel switch (Sw) was moved prior to the measurement, becoming a quantum channel switch, implemented by a nonpolarizing beam splitter acting as a local pick-off.

State characterization was done using a (tomographically complete) set of polarizing plates on a spinning wheel, while the compensating wave plates were placed in the main outgoing beam, all of which were located on the pointing stage at the transmitter. One interesting advantage of this approach is that only the optical pulse power exiting the transmitter telescope is relevant for QKD security, and thus any power lost to the polarization alignment pick-off can be compensated by increasing the WCP source power. This in turn implies that the pick-off power may be chosen independently of the power of the transmitted signal.

Because source emission continued regardless of the state of the alignment protocol, it was important to avoid position updates for the compensating wave plates that, as they moved, would cause lengthy excursions around the Poincaré sphere. This was done by adding a term to the cost function  $C$  proportional to the absolute change in positions of the wave plates, thereby limiting wave plate motion to “nearby” solutions that were clearly beneficial to the alignment of the transmitted signal states.

Figure 6 illustrates the active protocol in operation in a preliminary laboratory test. There, characterization of the unitary was performed using the first 10 000 de-

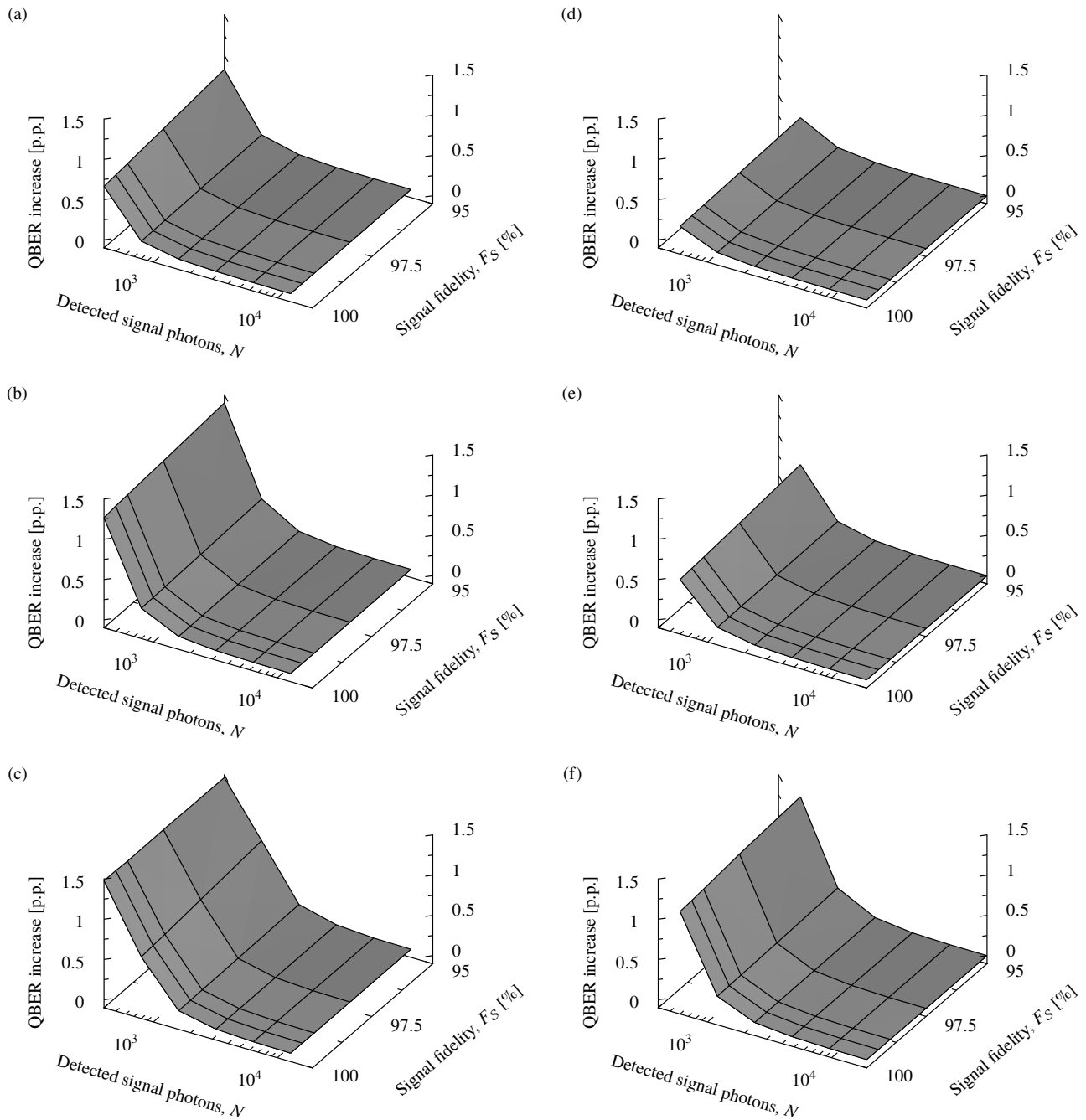


FIG. 4. Increase of the mean residual QBER of the protocol when using background subtraction, as compared to without subtracting the background. The left column shows results for the forward case with (a) 100, (b) 200, and (c) 400 mean background counts in each of its six detectors. The right column shows results for the reversed case with (d) 100, (e) 200, and (f) 400 mean background counts in each of its four detectors.

tection events for every second of data collected. Following coincidence analysis and tomographic reconstruction, the compensation wave plate orientations were optimized and applied. From this test complete correction to the intrinsic QBER of the source (approximately 6% to 7% at that time) was observed within a few seconds of inducing polarization disturbances by manipulating the input

fiber. The delay was predominately caused by the limited rotation speed of the compensation wave plate mounts (up to 2.25 seconds for the longest trip), combined with settling of the manipulated fiber, and the up-to 1-second delay inherent to the data collection.

Active polarization alignment was instrumental in performing QKD to the truck-mounted moving receiver.

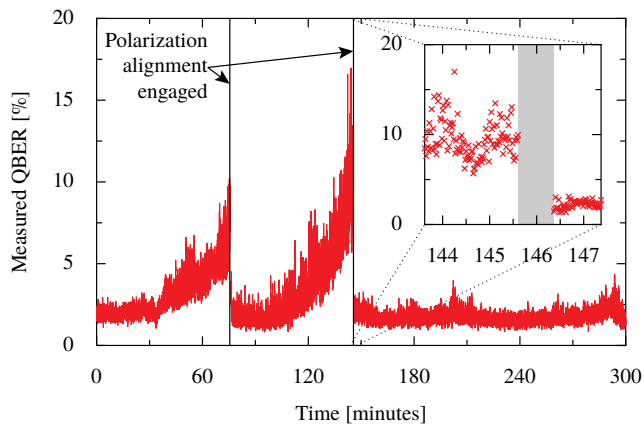


FIG. 5. Experimentally measured QBER of a 76 MHz QKD source. At the two points indicated, the polarization alignment protocol was engaged and the drifting QBER was brought back to the intrinsic level. The inset shows detail at the second instance; the shaded region indicates where the alignment protocol was operating (taking measurements and adjusting wave plate orientations).

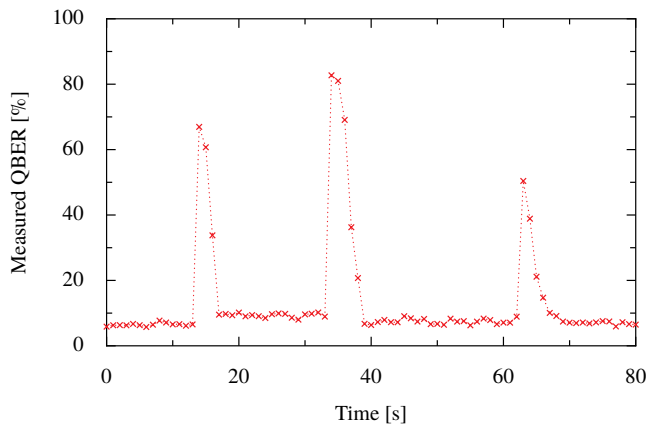


FIG. 6. Measured QBER (points) with automated application of the polarization alignment protocol, based on analysis of 10 000 detections each second. Dotted lines act as visual guides. Sudden increases in the QBER were caused by rapidly moving fiber polarization controller plates by hand, and were almost immediately corrected by the protocol—limited, primarily, by the speed of the rotating motors.

With  $\approx 4300$  detections each second, it maintained a received QBER of  $\approx 6\%$  (see Fig. 6 in Ref. [27], and discussion therein), very close to the intrinsic QBER of the source, and allowing positive key distillation. With no compensation, the QBER would have been  $\approx 12\%$  and yielded no key. A similar on-line compensation approach has also most recently been utilized in next-generation apparatuses—which include larger telescopes, integrated receiver optics, and a 400 MHz QKD-state source at 785 nm with intrinsic QBER of only  $\approx 1\%$ —to support a demonstration of QKD transmitted from the ground to an aircraft in flight [28].

## V. INITIALIZATION AND TIME CORRELATION

The polarization alignment protocol requires that photon detection events can be reliably correlated to source preparations. For stochastic sources, such as entangled-photon sources based on continuous-wave-pumped spontaneous parametric down-conversion, this timing alignment process can be based on correlating the random temporal differences between events. For pulsing sources, however, equivalent temporal differences may be seen for any number of multiple pulse period offsets. This could present a challenge for initialization of a WCP QKD device: if Alice and Bob observe an initially high QBER upon start-up, how can they know whether to try to correct the polarization, based on those results, or adjust their timing offsets, to possibly find different results?

Let  $\psi_a \in \{H, V, D, A\}$  be Alice’s choice of photon state preparation (assumed independent and with each state having equal likelihood), and  $\phi \in \{H, V, D, A\}$  be Bob’s measurement outcome. Suppose the timing is misaligned—i.e., tagged measurement outcomes do not correspond to source events. In this case, a photon thought to be prepared in state  $|\psi_a\rangle$  and subsequently received by Bob will instead have undergone an uncorrelated preparation to  $|\psi'_a\rangle$ , different from  $|\psi_a\rangle$  with 3/4 probability. The photon states that Bob measures, conditioned on each  $\psi_a$ , thus constitute an equally distributed sample of all four of Alice’s possible preparation choices, making the ensemble equivalent to a complete incoherent mixture. If Bob is able to measure the apparent purity of the received states (e.g., if he also measured in the  $R/L$  basis) then he could immediately distinguish this from high QBER caused by an unknown rotation  $\hat{U}$  (which does not introduce mixture).

Interestingly, Bob does not require those extra measurements to make such a distinction. Note that the detection probability of any measurement outcome  $\phi$  given this mixture is 1/4 (where we have included the random choice of basis). The application of a unitary operation  $\hat{U}$  prior to the measurement will have no effect on this mixed state, therefore we find

$$\Pr[\phi|\psi_a, \hat{U}] = \frac{1}{4} \quad \forall \phi, \psi_a, \hat{U}. \quad (2)$$

If, on the other hand, Bob’s detection events do correspond to Alice’s preparation events, then the application of  $\hat{U}$  will affect the probability of the measurement outcomes. By the following argument, in this case we find that

$$\max_{\phi, \psi_a} \Pr[\phi|\psi_a, \hat{U}] \geq \frac{3}{8} \quad \forall \hat{U}. \quad (3)$$

That is, for some combination of measurement outcome  $\phi$  and state preparation  $\psi_a$ , the detection probability will be at least 3/8. This means that, by collecting sufficient detection statistics in the four linear measurement



bases, it is possible to differentiate between misaligned timing and misaligned polarization regimes—the former will exhibit  $\approx 1/4$  detection frequency for any  $\phi$  and  $\psi_a$ , whereas, for some combination of  $\phi$  and  $\psi_a$ , the latter will exhibit  $\gtrsim 3/8$  detection frequency.

To see that this must be the case, consider the states lying on the Poincaré sphere in Bob’s polarization basis frame. Here, the four possible states for  $|\phi\rangle$  lie around the equator at  $90^\circ$  increments, and the four possible states for  $|\psi_b\rangle = \hat{U}|\psi_a\rangle$  lie around some great circle on the sphere, also at  $90^\circ$  increments. Our aim is to find the class of states  $\phi$  and  $\psi_a$  that maximizes the projection probability (equivalently, minimizes the angular distance), and then select a rotation  $\hat{U}$  to minimize this probability (maximize the angular distance)—this will constitute the limiting case in the inequality, Eq. (3).

First we simplify by reducing the size of the considered state space. If we consider a  $\hat{U}$  causing one  $|\psi_b\rangle$  state to lie at an angle  $\delta$  to a pole, then any adjacent  $|\psi_b\rangle$  state (from a different preparation) must lie at an angle at least  $90^\circ - \delta$  to the pole. If we have a  $|\psi_b\rangle$  with  $\delta < 45^\circ$  (i.e., closer to the pole than the equator), there will thus be another  $|\psi_b\rangle$  with  $\delta > 45^\circ$  (i.e., closer to the equator than the pole). As we need only consider the  $|\psi_b\rangle$  closest to the set of measurement states, which lie on the equator, we may therefore ignore the region beyond  $45^\circ$  above and below the equator, as states outside this region cannot be closest of all potential  $|\psi_b\rangle$  states to any  $|\phi\rangle$ .

Next, because of symmetry, we may also limit our considerations to the front hemisphere of the Poincaré sphere, as the rear hemisphere will exhibit equal projection probabilities for the set of corresponding opposite (orthogonal in Hilbert space) states. There will be at most two  $|\psi_b\rangle$  of relevance lying within the remaining hemispherical segment.

The positions farthest from any  $|\phi\rangle$  are those that lie equally distant from a pair of adjacent measurement states—i.e., positions on arcs of great circles on the Poincaré sphere, passing midway between  $|\phi\rangle$  states (see Fig. 7). We can satisfy these conditions for two  $|\psi_b\rangle$  states simultaneously, while maintaining their  $90^\circ$  separation, by choosing  $\hat{U}$  such that it places them at opposite ends of one such arc,  $\pm 45^\circ$  from the equator. The angle subtended from either of these positions to either nearby  $|\phi\rangle$  is  $60^\circ$ , thus the projection probability for both states is  $3/4$ .

Because the photons Bob receives will be measured in one of the two bases,  $H/V$  or  $D/A$ , with probability  $1/2$ , we finally arrive at the maximum detection probability, for some  $\phi$  and  $\psi_a$ , minimized over all possible rotations  $\hat{U}$ , of  $3/8$ .

## VI. DISCUSSION AND CONCLUSION

We have presented and experimentally implemented a polarization frame compensation protocol tailored to BB84 QKD, and theoretically characterized the photonic

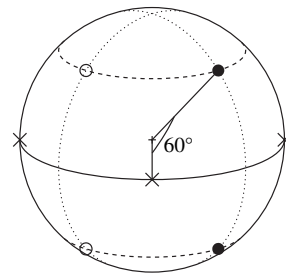


FIG. 7. Poincaré sphere representation of the possible locations of received states  $|\psi_b\rangle$  (circles) with respect to measurement states  $|\phi\rangle$  (crosses), where the projection probability has been minimized by  $\hat{U}$ . Open and closed circles each illustrate one possible configuration. Because of symmetries (see text), the extremal positions fall on the intersecting points of great circles which lie equidistant to adjacent measurements (dotted lines) with circles  $45^\circ$  above and below the equator (dashed lines). The angular distance of these positions, measured at the center of the sphere (indicated by the small plus), is  $60^\circ$ .

resources required for it to maintain good alignment. The protocol utilizes only the single-photon-level states of the BB84 protocol itself and state generation or state measurement that is tomographically complete (which can be achieved by making intelligent use of the wave plates necessary to compensate the observed polarization rotation). Given less than a few percent of recorded counts in a realistic scenario, the residual QBER is below source intrinsic QBER, even over high-loss links—for example, in any context where the signal fidelity is high enough to perform QKD, better than 1% residual QBER is possible in a single execution with only 400 detections. Thanks to this low resource requirement, the correction can be fast (within a few seconds), limited primarily by the physical reconfiguration of the compensation optics. Notably, many of the required counts could be extracted from detections assigned to parameter estimation—counts which are already destined to be excluded from the generated key.

As a comparison, by maintaining optimal reference frame alignment, active polarization correction allows BB84 protocols to achieve greater secure key rates than RFI QKD in the general case [14]. It should be noted that RFI QKD assumes one basis remains well-aligned, which is not the case for a general  $SU(2)$  unitary operation, and which the protocol presented here can naturally accommodate. Also interesting is that RFI QKD requires *random* selection out of three bases for each qubit measurement, as this is a part of the security model, whereas a polarization alignment procedure which does not impact the security model (because it applies identical compensation to all states) can safely perform the *same* measurement on multiple qubits in a row, for each basis.

If fast measurement basis switching is available, a polarization alignment protocol such as presented here may have an advantage in some regimes over polarimetry of

classical side-channel signals due to the time-scales involved. For example, with some practical polarimetry devices, fluctuating free-space links cause erratic results as the optical power fluctuates on time-scales similar to the rate of polarimetric measurements. With our protocol, randomly selected states at MHz pulse rates are transmitted far faster than free-space link intensity fluctuations occur, and thus the effects of these fluctuations wash out in the photon count statistics.

Clearly, our polarization alignment protocol is not quantum-mechanically optimal—for ensembles of identical preparations, optimal approaches must use collective treatments [29]. It is, however, sufficiently efficient and relatively simple to implement as to make it practically useful. Interestingly, there is a trade-off between the number of photons repurposed from key generation to perform the polarization alignment protocol, and the QBER achieved. An optimum must exist, as lower QBER increases the number of secure key bits that can be generated per received photon.

More generally, more sophisticated techniques could be incorporated into the protocol to make it more theoretically efficient or practically compact. For example, direct estimation of state fidelities [30] might provide a faster mechanism to assess whether full characterization and compensation is necessary. Or, where feasible, more

optimal measurement approaches (e.g., [24, 31]) or more compact polarimetry technologies (e.g., [32]) could potentially improve the practicality of the characterization apparatus. Other enhancements, such as estimators optimized for small-changes (e.g., [33]) or online optimum-seeking control mechanisms (e.g., [34]), with closed-loop control incorporating the compensation elements in the measurement, could be applied to the case of continuous polarization control.

Nevertheless, under the conditions of an orbiting satellite, this protocol, as it is, has the potential to sufficiently calibrate upon initial acquisition (or some time near it), and maintain calibration (by regular, possibly time-multiplexed, application of this protocol) throughout the remainder of the operating pass.

## VII. ACKNOWLEDGEMENTS

We thank Nikolay Gigov for helpful discussions and data processing of some experimental demonstrations. We thank NSERC, Canadian Space Agency, CFI, CIFAR, Industry Canada, FedDev Ontario, and Ontario Research Fund for funding. B.L.H. acknowledges support from NSERC Banting Postdoctoral Fellowships (Canada).

- 
- [1] Nicolas Gisin, Grégoire Ribordy, Wolfgang Tittel, and Hugo Zbinden, “Quantum cryptography,” *Rev. Mod. Phys.* **74**, 145–195 (2002).
  - [2] Valerio Scarani, Helle Bechmann-Pasquinucci, Nicolas J. Cerf, Miloslav Dušek, Norbert Lütkenhaus, and Momtchil Peev, “The security of practical quantum key distribution,” *Rev. Mod. Phys.* **81**, 1301–1350 (2009).
  - [3] C. H. Bennett and G. Brassard, “Quantum cryptography: Public key distribution and coin tossing,” in *Proceedings of the IEEE International Conference on Computers, Systems, and Signal Processing* (Bangalore, India, 1984) pp. 175–179.
  - [4] C. Bonato, A. Tomaello, V. Da Deppo, G. Naletto, and P. Villoresi, “Feasibility of satellite quantum key distribution,” *New J. Phys.* **11**, 045017 (2009).
  - [5] Evan R. Jeffrey, Joseph B. Altepeter, Madalina Colci, and Paul G. Kwiat, “Optical Implementation of Quantum Orienteering,” *Phys. Rev. Lett.* **96**, 150503 (2006).
  - [6] E. Bagan, M. Baig, A. Brey, R. Muñoz-Tapia, and R. Tarrach, “Optimal Strategies for Sending Information through A Quantum Channel,” *Phys. Rev. Lett.* **85**, 5230–5233 (2000).
  - [7] Asher Peres and Petra F. Scudo, “Entangled Quantum States as Direction Indicators,” *Phys. Rev. Lett.* **86**, 4160–4162 (2001).
  - [8] E. Bagan, M. Baig, and R. Muñoz-Tapia, “Communication of spin directions with product states and finite measurements,” *Phys. Rev. A* **64**, 022305 (2001).
  - [9] E. Bagan, M. Baig, and R. Muñoz-Tapia, “Aligning Reference Frames with Quantum States,” *Phys. Rev. Lett.* **87**, 257903 (2001).
  - [10] E. Bagan, M. Baig, and R. Muñoz-Tapia, “Quantum reverse engineering and reference-frame alignment without nonlocal correlations,” *Phys. Rev. A* **70**, 030301(R) (2004).
  - [11] Manuel A. Ballester, “Estimation of unitary quantum operations,” *Phys. Rev. A* **69**, 022303 (2004).
  - [12] Anthony Laing, Valerio Scarani, John G. Rarity, and Jeremy L. O’Brien, “Reference-frame-independent quantum key distribution,” *Phys. Rev. A* **82**, 012304 (2010).
  - [13] Vincenzo D’Ambrosio, Eleonora Nagali, Stephen P. Walborn, Leandro Aolita, Sergei Slussarenko, Lorenzo Marrucci, and Fabio Sciarrino, “Complete experimental toolbox for alignment-free quantum communication,” *Nature Comm.* **3**, 961 (2012).
  - [14] J. Wabnig, D. Bitauld, H. W. Li, A. Laing, J. L. O’Brien, and A. O. Niskanen, “Demonstration of free-space reference frame independent quantum key distribution,” *New Journal of Physics* **15**, 073001 (2013).
  - [15] Liang Wen-Ye, Wen Hao, Yin Zhen-Qiang, Chen Hua, Li Hong-Wei, Chen Wei, and Han Zheng-Fu, *Comm. Theor. Phys.* **64**, 295 (2015).
  - [16] G. B. Xavier, G. Vilela de Faria, T. Ferreira da Silva, G. P. Temporão, and J. P. von der Weid, “Active polarization control for quantum communication in long-distance optical fibers with shared telecom traffic,” *Micro. Opt. Tech. Lett.* **53**, 2661–2665 (2011).
  - [17] M. Sasaki, M. Fujiwara, H. Ishizuka, W. Klaus, K. Wakui, M. Takeoka, S. Miki, T. Yamashita, Z. Wang, A. Tanaka, K. Yoshino, Y. Nambu, S. Takahashi, A. Tajima, A. Tomita, T. Domeki, T. Hasegawa, Y. Sakai, H. Kobayashi, T. Asai, K. Shimizu, T. Tokura,

- T. Tsurumaru, M. Matsui, T. Honjo, K. Tamaki, H. Takesue, Y. Tokura, J. F. Dynes, A. R. Dixon, A. W. Sharpe, Z. L. Yuan, A. J. Shields, S. Uchikoga, M. Legré, S. Robyr, P. Trinkler, L. Monat, J.-B. Page, G. Ribordy, A. Poppe, A. Allacher, O. Maurhart, T. Länger, M. Peev, and A. Zeilinger, “Field test of quantum key distribution in the Tokyo QKD Network,” *Opt. Express* **19**, 10387–10409 (2011).
- [18] Any significant polarization-sensitive non-unitary effect would be inherently detrimental to the quantum bit error rate (QBER), preventing successful QKD over that channel regardless of relative frame alignment.
- [19] Alternately, if Alice has an entangled photon source as for the BBM92 protocol, she may measure her photon in order to project Bob’s photon onto the  $|H\rangle$ ,  $|V\rangle$ ,  $|D\rangle$ , and  $|A\rangle$  states, again just as she would do for the QKD protocol.
- [20] William K. Wootters and Brian D. Fields, “Optimal State-Determination by Mutually Unbiased Measurements,” *Ann. Phys.* **191**, 363–381 (1989).
- [21] Z. Hradil, J. Summhammer, G. Badurek, and H. Rauch, “Reconstruction of the spin state,” *Phys. Rev. A* **62**, 014101 (2000).
- [22] Although we do not directly reconstruct  $\hat{U}$ , in principle the inverse of  $\hat{V}(\theta)$  will be a close approximation. However, only the angles in  $\theta$  are necessary to physically implement the compensation.
- [23] J.-P. Bourgoin, E. Meyer-Scott, B. L. Higgins, B. Helou, C. Erven, H. Hübel, B. Kumar, D. Hudson, I. D’Souza, R. Girard, R. Laflamme, and T. Jennewein, “A comprehensive design and performance analysis of low Earth orbit satellite quantum communication,” *New J. Phys.* **15**, 023006 (2013).
- [24] Jaroslav Řeháček, Berthold-Georg Englert, and Dagomir Kaszlikoski, “Minimal qubit tomography,” *Phys. Rev. A* **70**, 052321 (2004).
- [25] Jean-Philippe Bourgoin, Nikolay Gigov, Brendon L. Higgins, Zhizhong Yan, Evan Meyer-Scott, Amir K. Khandani, Norbert Lütkenhaus, and Thomas Jennewein, “Experimental quantum key distribution with simulated ground-to-satellite photon losses and processing limitations,” *Phys. Rev. A* **92**, 052339 (2015).
- [26] Z. Yan, E. Meyer-Scott, J.-P. Bourgoin, B. L. Higgins, N. Gigov, A. MacDonald, H. Hübel, and T. Jennewein, “Novel high-speed polarization source for decoy-state BB84 quantum key distribution over free space and satellite links,” *J. Lightwave Technol.* **31**, 1399 (2013).
- [27] Jean-Philippe Bourgoin, Brendon L. Higgins, Nikolay Gigov, Catherine Holloway, Christopher J. Pugh, Sarah Kaiser, Miles Cranmer, and Thomas Jennewein, “Free-space quantum key distribution to a moving receiver,” *Opt. Express* **23**, 33437 (2015).
- [28] Christopher J. Pugh, Sarah Kaiser, Jean-Philippe Bourgoin, Jeongwan Jin, Nigar Sultana, Sascha Agne, Elena Anisimova, Vadim Makarov, Eric Choi, Brendon L. Higgins, and Thomas Jennewein, “Airborne demonstration of a quantum key distribution receiver payload,” *Quantum Sci. Technol.* **2**, 024009 (2017).
- [29] S. Massar and S. Popescu, “Optimal Extraction of Information from Finite Quantum Ensembles,” *Phys. Rev. Lett.* **74**, 1259–1263 (1995).
- [30] Steven T. Flammia and Yi-Kai Liu, “Direct Fidelity Estimation from Few Pauli Measurements,” *Phys. Rev. Lett.* **106**, 230501 (2011).
- [31] Alexander Ling, Kee Pang Soh, Antía Lamas-Linares, and Christian Kurtsiefer, “An optimal photon counting polarimeter,” *J. Mod. Opt.* **53**, 1523–1528 (2006).
- [32] S. Gupta Roy, O. M. Awartani, P. Sen, B. T. O’Connor, and M. W. Kudenov, “Intrinsic coincident linear polarimetry using stacked organic photovoltaics,” *Opt. Express* **24**, 14737–14747 (2016).
- [33] P. Kolenderski and R. Demkowicz-Dobrzanski, “Optimal state for keeping reference frames aligned and the platonic solids,” *Phys. Rev. A* **78**, 052333 (2008).
- [34] J. Fisher, A. Kodanev, and M. Nazarathy, “Multi-degree-of-freedom stabilization of large-scale photonic-integrated circuits,” *J. Lightwave Technol.* **33**, 2146–2166 (2015).